

# The paradoxical behavior of rough colloids at fluid interfaces

Md Anisur Rahman and Peter J. Beltramo\*

Department of Chemical Engineering, University of Massachusetts Amherst, Amherst, Massachusetts 01003, USA

**ABSTRACT:** Colloidal particles adsorb and remain trapped at immiscible fluid interfaces due to strong interfacial adsorption energy, with a contact angle defined by the chemistry of the particle and fluid phases. An undulated contact line may appear due to either particle surface roughness or shape anisotropy, which results in a quadrupolar interfacial deformation and strong long range capillary interaction between neighboring particles. While each effect has been observed separately, here we report the paradoxical impact of surface roughness on spherical and anisotropic ellipsoidal polymer colloids. Using a seeded emulsion polymerization technique, we synthesize spherical and ellipsoidal particles with controlled roughness magnitude and topography (concave/convex). Via *in situ* measurement of the interfacial deformation around colloids at an air-water interface, we find that while surface roughness strengthens the quadrupolar deformation in spheres as expected by theory, in stark contrast, it weakens the same in ellipsoids. As roughness increases, particles of both shapes become more hydrophilic and their apparent contact angle decreases. Using numerical predictions, we show that this partially explains the decreased interfacial deformation and capillary interactions between ellipsoids. Therefore, particle surface engineering has the potential to decrease the capillary deformation by asymmetric particles via changing their capillary pinning as well as wetting behavior at fluid interfaces.

**KEYWORDS:** *polymer colloids, rough particles, fluid interfaces, capillarity, anisotropic colloids, interfacial phenomena, surface topography*

## INTRODUCTION

The irreversible pinning of polymer colloids to immiscible fluid-fluid interfaces can be exploited in designing a wide range of interfacial materials and processes, from stabilizing Pickering emulsions and foams to the bottom-up fabrication of two-dimensional (2D) microstructures<sup>1-4</sup>. Among various interparticle interactions between colloids at the interface which contribute to collective interfacial microstructure and properties, attractive capillary interactions are significant and originate from curved menisci around the particle<sup>5</sup>. In particular, far-field quadrupolar interfacial deformation<sup>6,7</sup> results from introducing either particle surface roughness in otherwise smooth spheres<sup>5</sup> or shape anisotropy as in ellipsoids<sup>8</sup>. The former originates from nanoscale random undulations in the contact line, which decays to a quadrupolar curved menisci, while the latter is a consequence of Young's law requiring constant three-phase contact angle around an object with varying curvature.<sup>6,7</sup> While theoretical predictions of roughness causing local contact line pinning undulations that scale to a quadrupolar deviation in the far field date back to 2000<sup>5,9</sup>, and its impact on emulsions observed shortly thereafter<sup>10</sup>, it was only in 2017 that gel-trapping was used to perform *ex situ* measurements

of the deformation to confirm<sup>11</sup>. On the other hand, *in situ* measurement of the quadrupolar interfacial deformation around smooth ellipsoids<sup>12,13</sup> and its impact on interfacial mechanics<sup>14,15</sup> is well documented.

Regardless of source, these deviations from a planar interface are energetically unfavorable due to increasing contact area between the immiscible fluids, and as a result strong, directionally dependent, interparticle capillary attraction arises. Due to the strong capillary force, anisotropic particles tend to form disordered multiparticle aggregates.<sup>14</sup> Increasing aggregation via roughness or particle shape is in some instances beneficial, where for instance foams and emulsions can be stabilized to a higher degree with less particles<sup>15,16</sup> and tuning emulsion stabilization is possible<sup>10,11</sup>. In contrast, applying Langmuir-Blodgett<sup>17</sup> techniques to assemble ordered arrays of particles for photonics applications<sup>18,19</sup> fails when applied to anisotropic particles due to the disorder that strong capillary interactions promote, which poses a significant barrier restricting their application in creating functional self-assembled materials. However, recently we discovered that adding roughness to polymeric ellipsoids decreases the magnitude of interfacial deformation<sup>7</sup>, which warrants further investigation into how different surface geometry induced roughness influences the interfacial pinning and deformation behavior by polymeric spheres and ellipsoids.

To that end, this work reports a systematic study of the effect of surface roughness and shape on the capillary pinning of polymer colloids. Spheres and ellipsoids with controlled surface topography (convex/concave) and roughness are synthesized and their interfacial pinning quantified via *in situ* Mirau interferometry. While we find that increasing roughness increases the magnitude of the capillary quadrupole around spheres, in accordance with theory, roughness decreases the capillary quadrupole between ellipsoids. To understand this discovery, we analyze the height of the particle at the interface and the apparent contact angle. We find that changes in contact angle may explain in part the decrease in interfacial capillary interactions between rough ellipsoids.

## RESULTS AND DISCUSSION

### Model Rough Spheres and Ellipsoids

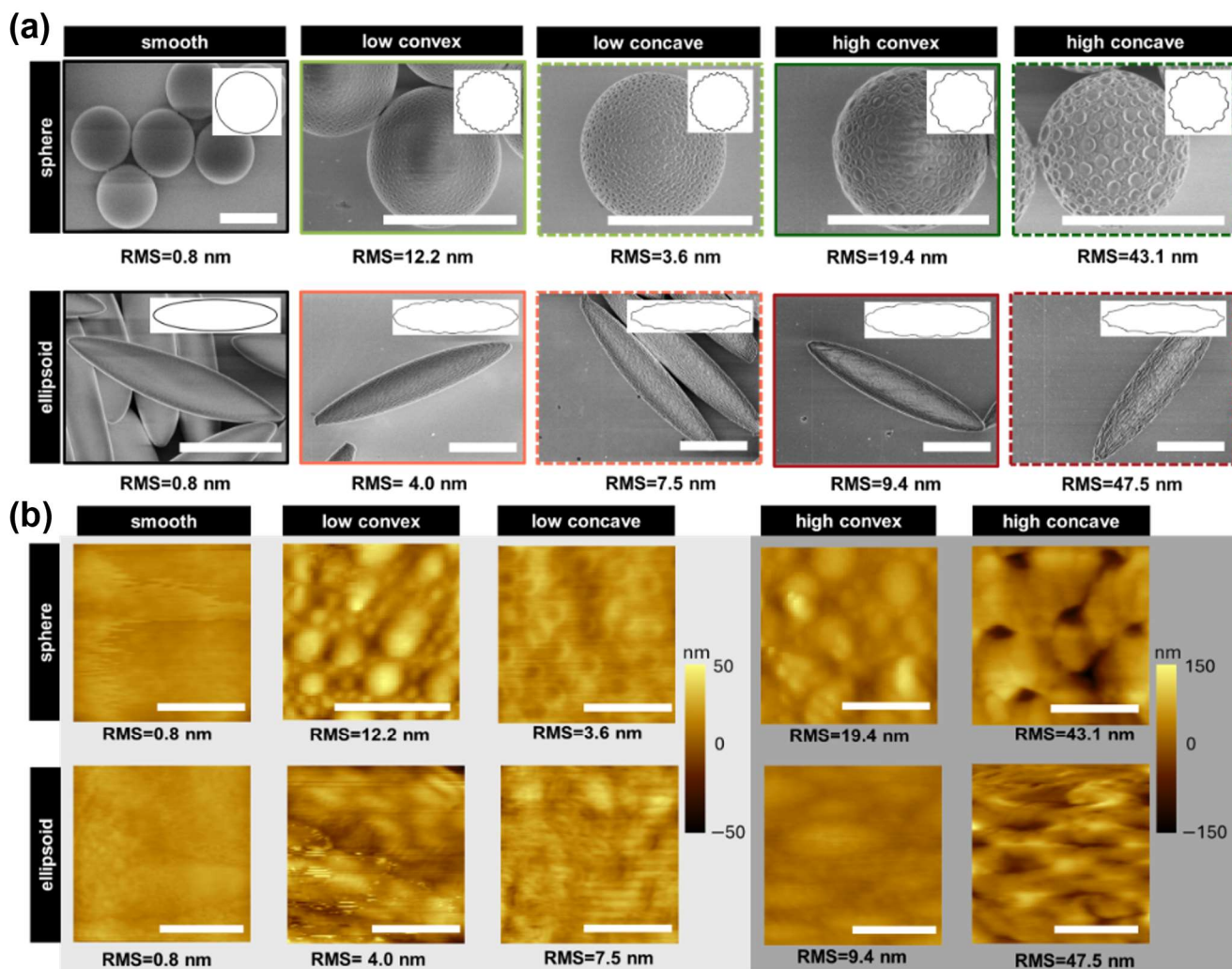


Figure 1. a) SEM and b) AFM images and corresponding RMS roughness values of model convex and concave rough microspheres and microellipsoids along with their smooth analogues. Ellipsoids have a 4.5:1 aspect ratio and are stretched from the convex spheres above. Scale bars represent 5  $\mu\text{m}$  for SEM and 1  $\mu\text{m}$  for AFM. AFM images are of the surface of the particle post particle curvature subtraction.

To examine the impact of particle surface roughness on the capillary pinning of shape isotropic and anisotropic polymeric particles, we have synthesized a suite of model colloids with two shapes ( $\sim 4$   $\mu\text{m}$  spheres and 4.5:1 aspect ratio ellipsoids), three degrees of roughness (0.8 – 47.5 nm RMS), and two types of surface roughness topography (convex/concave), following the procedure outlined in our previous work<sup>20,21</sup> and described in the Materials & Methods to produce polystyrene/poly(tert-butyl acrylate) (PS/PtBA) particles. Figure 1a shows SEM images of the synthesized rough microspheres and microellipsoids along with their smooth counterparts and the corresponding RMS roughness values. We note that due to minor beam damage to the PtBA domains, the SEM imaging does not accurately reflect the surface topography of the particles. AFM analysis of the particles quantitatively evaluates the true surface topography of the particles, showing that the roughness is successfully controlled over a range of 0.8 nm to 47.5 nm with both convex and concave features (Figure 1b). Upon stretching the convex particles into convex microellipsoids, the roughness decreases slightly due to the relative stretching and flattening of the protrusion from the particle surface. Concave particles are produced by performing acid catalyzed hydrolysis (ACH) to remove the PtBA bumps from the convex particles. Similar to our earlier report<sup>20</sup>, for relatively small bumps on the spherical particle surface (low convex), per-

forming ACH decreases the roughness since the PtBA domain is not symmetric at the particle interface (in this regime it protrudes out more than it deepens into the particle). In other cases, the ACH process increases the roughness of the particle.

#### Interfacial Deformation and Interaction Energy

The 10 particle types shown in Figure 1 are deposited at an air-water interface and their interfacial pinning characteristics evaluated *in situ* using Mirau interferometry<sup>13</sup> to measure the nanoscale fluid deformation surrounding isolated particles. Figure 2a shows exemplary relative height maps of the interface obtained from the interferograms for microspheres and microellipsoids with varying particle surface roughness. The fluid interface surrounding the smooth sphere shows negligible deformation, while the smooth ellipsoid shows quadrupolar deformation, aligning with prior theory<sup>5,22</sup> and experiments<sup>11,12</sup>. The rough microspheres distort the fluid interface in the expected quadrupolar fashion with orthogonal dips and rises that becomes more pronounced as roughness increases, confirming prior *ex situ* results<sup>11</sup>. In stark contrast to the rough microspheres, the magnitude of the quadrupolar deformation observed in microellipsoids diminishes with increasing roughness. Figure 2bc shows the rise and dip profile of the water phase from the three-phase contact line extending from the particles. The height of the interface,  $h$ , decays as  $h \propto r^{-2}$  for both

rough spheres and smooth and rough ellipsoids, validating the quadrupolar nature of the interface deformation as predicted by capillary theory<sup>5</sup>. As observed qualitatively in the interferograms, the magnitude of the interfacial dip/rise increases with roughness for spheres, but decreases with roughness for ellipsoids. The capillary attraction between either a rough sphere or ellipsoid causing a quadrupolar interfacial deformation can be described by the following equation<sup>5,22</sup>:

$$U_{\text{cap}} = -3\pi\gamma_{12}\Delta h_{\text{max}}^2 \cos[2(\omega_1 + \omega_2)] \left(\frac{r_c}{r}\right)^4 \quad (1)$$

Here,  $\gamma_{12}$  is the surface tension at air-water interface,  $\omega_{1/2}$  denotes the in-plane orientation of the two particles with respect to their center-to-center distance,  $r$ , and  $r_c$  is the contact radius. From the interferometry, we directly measured the maximal height difference along the contact line ( $\Delta h_{\text{max}}$ ). The data gathered from at least five particles of each kind are compiled in Figure 2d. With an increase in surface roughness, the  $\Delta h_{\text{max}}$  increases for both types of rough microspheres, with the effect being more pronounced in concave spheres. In contrast,  $\Delta h_{\text{max}}$  diminishes in microellipsoids with surface roughness, with concave roughness again exhibiting a stronger effect. Therefore, while the dependence of interfacial deformation magnitude varies with roughness depending on the particle shape, the specific particle surface geometry (concave or convex) has a secondary influence on the interfacial pinning. We note that while each particle is imaged at least 15 minutes after deposition, changes of the metastable pinning dynamics could be enhanced and vary with surface topography, as observed with smooth spheres and ellipsoids<sup>23,24</sup>. Figure 2e reports the predicted  $U_{\text{cap}}$  values by applying Eqn 1 to our data and assuming mirror symmetric configuration of the particles. Vertical lines denote  $r_c$ , the radius of the spheres, and the particle separation at contact for ellipsoids in a side-side and tip-tip configuration. Since  $U_{\text{cap}}$  mostly depends on the  $\Delta h_{\text{max}}$ , a comparable dependency on particle surface heterogeneity and geometry from our discussion of Fig 2d is observed.

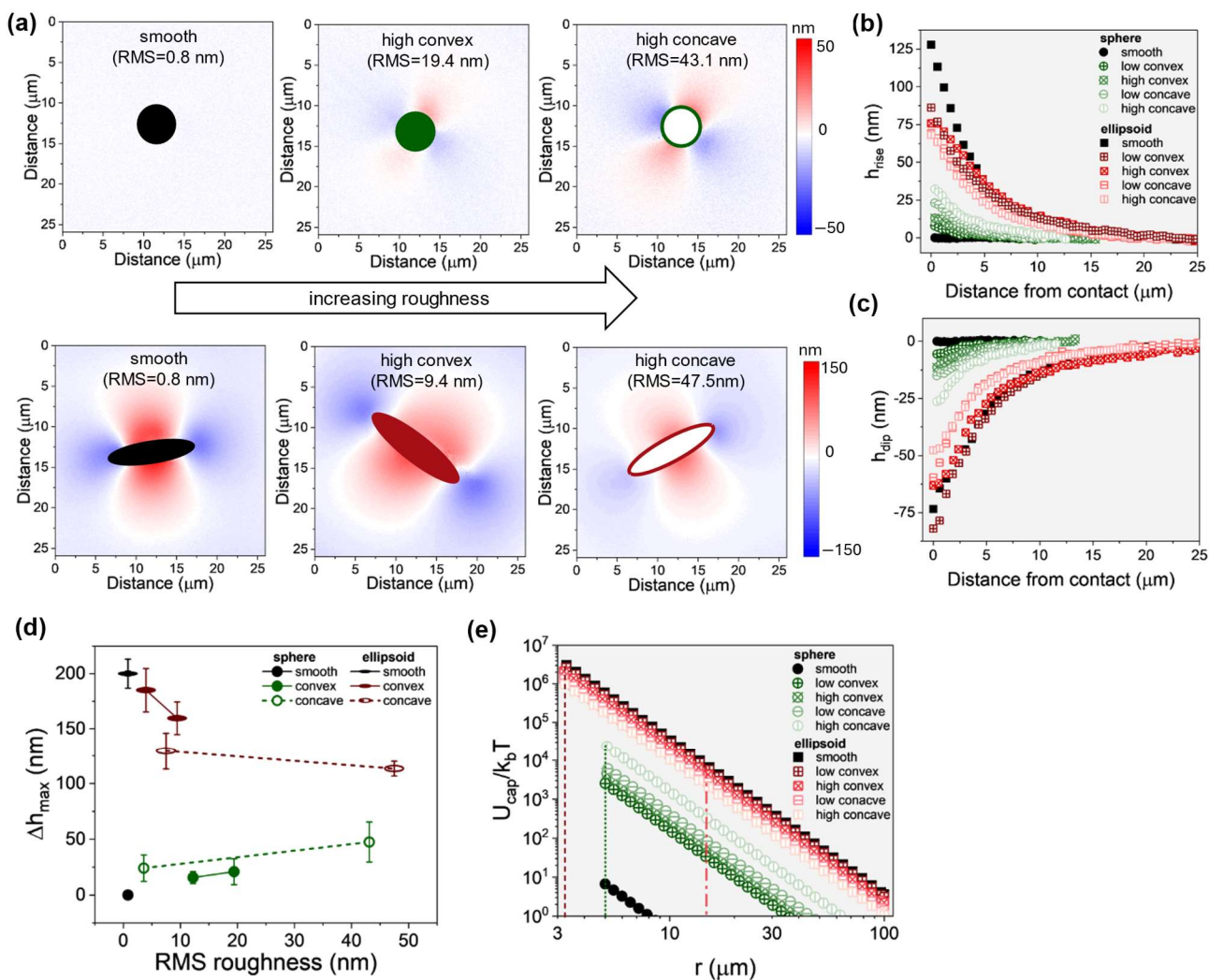


Figure 2. (a) Relative height map showing interfacial deformation around smooth, convex, and concave microparticles (top row-spheres and bottom row-ellipsoids) at an air-water interface. (b) The rise and (c) dip of the quadrupolar interfacial deformation as a function of distance from three phase contact point for all particle types. (d) Average interfacial deformation magnitude,  $\Delta h_{max}$ , showing the paradoxical behavior between spheres and ellipsoids which manifests in (e) the capillary attraction energy.

To gain insight into how roughness is causing disparate effects on the capillary interaction energy between spheres and ellipsoids, we further analyze the interferograms to determine the vertical position of the particle at the interface<sup>12,25</sup> and calculate the ratio of apparent projected area,  $S$ , occupied by the particle contour in the  $xy$ -plane of the interface to the total projected area,  $S_0$ , of the particle in the neutrally wetting condition (contact angle,  $\theta_c=90^\circ$ , ellipsoid lying in the plane of the interface). A value of  $S/S_0 < 1$  means the particle is hydrophilic, sitting more into the water sub-phase. Figure 3a shows as surface roughness increases,  $S/S_0$  decreases for both spheres and ellipsoids, with a more pronounced decrease for concave particles. This is consistent with complementary experiments on gel-trapped particles which also show particles becoming more immersed in the aqueous phase with increasing roughness (Figure 3d).

Apart from particle position,  $S/S_0$  can be combined with the interfacial deformation to calculate the apparent contact angle,  $\theta_{c,app}$ <sup>13</sup>. We denote this as an apparent particle contact angle since, in analogy to measuring contact angles on non-smooth surfaces, the actual nanoscopic pinning at the fluid-solid interface is difficult to resolve<sup>26</sup>. From Figure 3b, it is obvious that for both

spheres and ellipsoids the  $\theta_{c,app}$  decreases with an increase in roughness. We observe that for a particle with similar surface chemistry and roughness, the contact angle is smaller for ellipsoids than spheres, consistent with previous work on smooth particles by us<sup>13</sup> and by others<sup>12,27</sup>. We note that the scale of Figure 2b shows changes in height of  $\sim 10 - 100$  nm over  $\sim 1 - 10$   $\mu$ m distance from the particle. Therefore, the slope of the interface at the three-phase contact point changes minimally, implying that the change in  $\theta_{c,app}$  is mostly due to the slope of particle at the contact, which in turn is governed by the particle's height at the interface ( $S/S_0$ , Fig 3a).

The observation that the particles become more hydrophilic with increasing surface roughness agrees with numerical calculations of the minimum interfacial pinning energy of spheres with rough surfaces<sup>28,26</sup>. In the Wenzel wetting regime, as the particle surface area increases, the surface energy between the particle and fluid phases changes to shift the three-phase contact line such that the contact area between the particle and the fluid phase it wets more preferably increases. We also note that stretching a sphere into ellipsoid while keeping volume constant also enhances the surface area of ellipsoids relative to spheres, explaining the ten-

endency for ellipsoids to show smaller contact angles compared to spheres.

However, if we compare the  $\Delta h_{max}$  as a function of  $S/S_0$ , we see an opposite trend between spheres and ellipsoids (Figure 3c). For ellipsoids, a proportional relationship between  $\Delta h_{max}$  and  $S/S_0$  can be drawn. This indicates that incorporating  $S/S_0$  as a prefactor in Equation 1 can roughly estimate the  $\Delta h_{max}$  for rough ellipsoids given that the  $\Delta h_{max}$  of smooth ellipsoids is known, but as discussed next, the increasing hydrophilicity of rough ellipsoids only partially accounts for the pinning behavior.

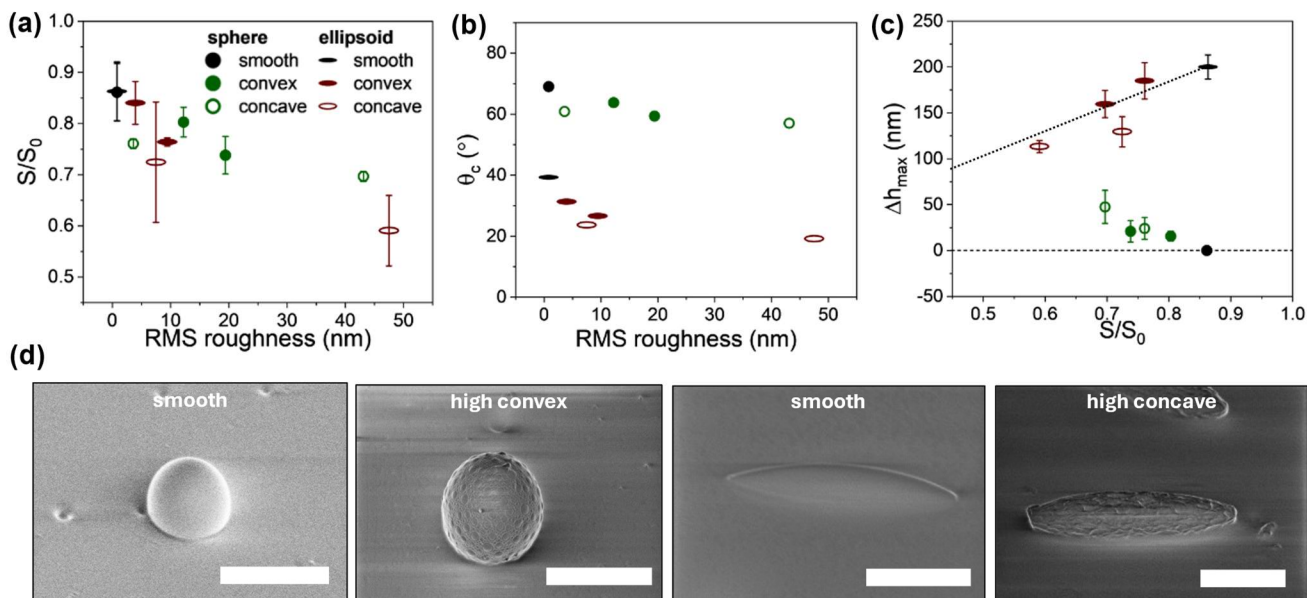


Figure 3. (a) Ratio of projected area enclosed by the contact line to that of a neutrally wetting particle ( $S/S_0 = 1$ ,  $\theta_c = 90^\circ$ ) and (b) apparent contact angle decreases with increasing roughness. (c) However,  $\Delta h_{max}$  increases for spheres but decreases for ellipsoids as a function of  $S/S_0$ . (d) Gel-trapping confirms the increase in particle hydrophilicity with roughness (note the “solid” surface below the particle was previously the air phase). All scale bars represent 5  $\mu\text{m}$ .

### Comparison to Theory

Although experimental evidence has shown a decrease in contact angle with increasing RMS roughness for inorganic silica spheres<sup>11</sup>, such observation for rough anisotropic particles has not previously been reported, which has significant implications on the contrasting behavior in  $\Delta h_{max}$  exhibited by rough ellipsoids. Using finite-element calculations, Dasgupta et al<sup>25</sup> showed that the  $\Delta h_{max}$  of ellipsoids increases with increasing  $\theta_c$ , attains a maximum value, and finally diminishes to zero for  $\theta_c = 90^\circ$ . A similar  $\theta_c$  dependency of  $\Delta h_{max}$  for ellipsoids has been reported by Lehle et al<sup>22</sup> using multipole expansions and Loudet et al<sup>12</sup> using boundary element methods. In Figure 4, we have summarized the  $\Delta h_{max}$  values as a function of  $\theta_c$  obtained from this work and compared them with analytically determined values. It is important to note that Loudet et al<sup>12</sup> observed the experimental  $\Delta h_{max}$  values to be smaller than those calculated numerically, and likewise we have scaled down the numerical prediction by a factor of four to align with our experimental findings. The data follow the general trend and lie on the left wing of the peak values of  $\Delta h_{max}$ . The  $\Delta h_{max}$  for smooth ellipsoids is close to the peak value corresponding to an aspect ratio of 4. If changes to the apparent contact angle of the particle were the only contribution altering the interfacial pinning characteristics, one would expect the data to continue to fall on the 4:1 aspect ratio curve. However, as contact angle decreases the experimental data shift from the curve for 4:1 aspect ratio to being closer to a 2.5:1 aspect ratio particle. This indicates that the decrease in  $\Delta h_{max}$  with roughness cannot only be ex-

plained by the decreasing contact angle, but in addition nanoscale surface roughness causes the particle to appear to have a lower aspect ratio at the interface.

We include the data on spherical particles in Figure 4 to highlight the potential for combining particle shape and surface roughness to tune interfacial capillary interactions. Slightly asymmetric particles may still exhibit increases in quadrupolar deformation with roughness, and perhaps a particle shape can be found where the effect of changing contact angle is perfectly offset by roughness effects to produce a particle whose capillary interactions are constant and independent with roughness. For larger aspect ratio ellipsoids, increasing roughness makes the particle behave more like a sphere, masking in part the microscopic particle curvature from dictating the contact line. Therefore, the capillary interaction energy between particles can potentially be tuned and decoupled from particle shape by integrating roughness into spherical particles or ellipsoids to increase and decrease the interactions, respectively.

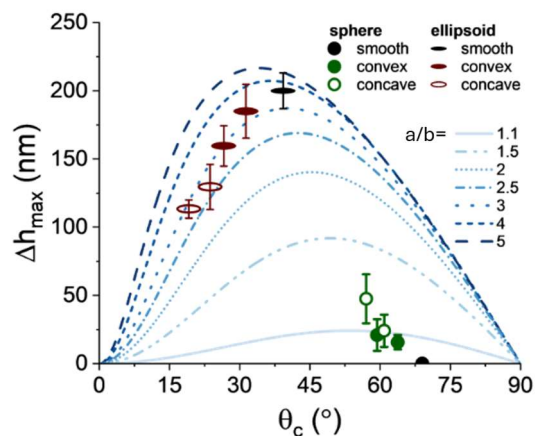


Figure 4.  $\Delta h_{max}$  as a function of apparent contact angle,  $\theta_c$ , for ellipsoids and spheres. Lines indicate calculations of the expected interfacial deformation at varying aspect ratio as described in the text.

## CONCLUSIONS

In summary, via *in situ* measurements of the interfacial deformation surrounding colloids pinned to air-water interfaces, we have shown how surface roughness dictates the interfacial pinning and capillary interactions of spheres and ellipsoids. While roughness strengthens the quadrupolar deformation in spheres, as expected from theory, it remarkably and unexpectedly weakens it for ellipsoids. The added benefit of introducing surface heterogeneity to shape-anisotropic ellipsoids is to alter their capillary pinning behavior that in turn decreases the  $\theta_c$  as well as the  $\Delta h_{max}$ , partially aligning with the numerical predictions. These findings, which can potentially be extended to different shaped asymmetric particles, open up the opportunities to tune interfacial interaction, mechanics, and assembly of such colloids at fluid interfaces via particle surface engineering. This can aid in engineering fluid-fluid interface stability in emulsions and foams and realizing complex 2D ordered microstructures from anisotropic particles by leveraging rational control over the interparticle interaction energy.

## MATERIALS AND METHODS

### Materials

Styrene (Sigma-Aldrich, 99%), poly(vinylpyrrolidone) (PVP, Sigma-Aldrich, 40,000 g/mole), azobisisobutyronitrile (AIBN, Sigma-Aldrich, 99%), isopropyl alcohol (IPA, Fisher Scientific, Certified ACS,  $\geq 99.5\%$ ), ethanol (EtOH, Fisher Scientific, Certified ACS, 95%) tertbutyl acrylate (tBA, Aldrich, 98%), 2,2'-azobis(2,4-dimethylvaleronitrile) (Wako V-65,  $>95\%$ ), poly(vinyl alcohol) (PVA, Sigma-Aldrich, 13,000–23,000 g/mole, 87–89% hydrolyzed), trifluoroacetic acid (TFA, Sigma-Aldrich, 99%), gellan gum (GG, Thermo Scientific), and Sylgard 184 curable silicone elastomer (poly(dimethylsiloxane) (PDMS), Dow Chemical Company) were used as received. Ultrapure deionized water (DI, resistivity  $> 18.2$  M $\Omega$ -cm, Millipore Milli-Q) was used for aqueous solution preparation and particle washing.

### Particle Synthesis

LPS seed particles were first synthesized by dispersion polymerization. 0.36 g PVP was added to 18.4 mL IPA in a 50 mL round bottom flask (RBF). 0.05 g of oil soluble initiator,

AIBN, was dissolved in 5.6 mL of styrene monomer in a separate glass vial, and the resulting solution was added to the RBF. The solution in the RBF was purged with nitrogen for 5 minutes and then rotated in a 70°C oil bath for 24 hours to ensure complete polymerization. After polymerization, the particles were washed thoroughly with water by at least five alternating centrifugation and sonication steps. The resultant smooth LPS spheres were either stretched to form smooth ellipsoids (details below) or further processed into convex spheres by seeded emulsion polymerization (SEP).

For synthesizing low (high) roughness convex spheres using SEP, first, a monomer mixture of 0.2 (0.3) mL tBA and 2.5 (5) wt% of V-65 initiator was made in a 7.1 mL glass vial. Next, 3.2 mL of 1 wt% aqueous PVA solution was added, followed by vortexing for 60 seconds to form an emulsion before 0.3 g LPS seed spheres suspended in 0.8 mL of 1 wt% aqueous PVA solution were added. The vial was then rotated at 30 rpm for 24 hours to facilitate the swelling of the seed spheres with the monomer mixture. Polymerization was then carried out by placing the seeded emulsion vial in a 70°C oil bath and rotating at 40 rpm for 24 hours. Convex spheres were recovered by washing with water by alternating centrifugation and sonication for at least six times. These particles were either stretched to form convex ellipsoids or further processed into concave spheres by acid catalyzed hydrolysis (ACH, details below).

Polymer microspheres were stretched into 4.5:1 aspect ratio microellipsoids using our established method<sup>21</sup>. Briefly, smooth or convex microspheres were spread on a PVA solution in a Teflon template and allowed to dry. The dried particle embedded film was loaded onto the stretching apparatus and heated in an oil bath to  $T = 115$  °C, before being stretched to a predetermined draw ratio (2:1). The stretched PVA film was cut to isolate regions with the desired aspect ratio particles then dissolved in water to recover the particles. At least six consecutive centrifugation-resuspension cycles were then carried out to recover smooth or convex ellipsoids.

ACH was performed to remove the convex patch (PtBA) domains from the spheres and ellipsoids by converting the domains to water-soluble poly(acrylic acid). 3 mL of TFA was added to a glass vial containing 100 mg of PS-PtBA particles centrifuged out from a water suspension and was placed under magnetic stirring for 24 hours. Afterwards, the particles were washed at least five times by alternating centrifugation and sonication, with the first wash performed after adding EtOH to adjust the fluid phase density and all subsequent washes performed using water.

### Particle Characterization

Scanning electron microscopy (SEM) images were obtained using an FEI Magellan 400 XHR scanning electron microscope operating at acceleration voltage of 1 kV. The SEM samples were prepared via drop casting the particle suspension in water onto silicon wafer chips followed by drying at ambient conditions. The particles were imaged without a conductive metal coating. Using ImageJ, the diameters of the particles were measured by analyzing SEM images of  $>100$  particles. The patch diameter was determined by measuring at least 200 patches spread across no less than 10 particles. Minor beam damage on the PtBA domains prevents quantitative analysis of the surface topography via SEM, in particular making convex particles appear to have concave features.

Therefore, the surface roughness of the produced particles was measured by scanning a single particle via atomic force microscopy (AFM). Prior to AFM, the particles were immobilized on a PDMS film using gel trapping<sup>29</sup>. In brief, a 2 wt% suspension of GG was prepared by adding the required amount of GG powder to DI water at 80 °C under continuous stirring at 1200 rpm for 2 h. 5

mL of 0.1 wt% particle suspension in water/EtOH (equal volume) were spread at the air-GG interface prepared by pouring GG solution into a 35 mm glass Petri dish. The samples were allowed to cool down to room temperature to jelly the aqueous GG phase and thus trap the particles at the interface. PDMS was manually mixed with the curing agent in a 10:1 ratio and centrifuged at 4000 rpm for 15 min to remove all the gas bubbles that evolved from the mixing. Next, the gelled aqueous phase was carefully covered by PDMS elastomer and allowed to cure for 48 h at room temperature. The PDMS film containing the trapped particles was washed several times in water to remove any remaining GG from the particle surface. Root-mean-square (RMS) roughness of the trapped particles was measured via AFM imaging on a single particle using an Asylum MFP-3D. Tapping mode images were acquired via probing the sample surface with an Olympus AC240TS-R3 silicon cantilever having a spring constant of  $2 \text{ Nm}^{-1}$  and a resonance frequency of 70 kHz at ambient condition. The open-source software Gwyddion<sup>30</sup> was used to analyze the obtained images. To obtain RMS values, the macroscopic particle curvature was subtracted to obtain the residual surface height profile<sup>20,31</sup>, from which the RMS roughness was calculated. The RMS values and its standard deviation were calculated from a minimum of five particles for each sample by measuring at least two regions of  $1.5 \mu\text{m}$  by  $1.5 \mu\text{m}$  area on each particle.

### Interferometry

A suspension containing 0.1% particles by weight in water is mixed with  $5 \mu\text{L}$  IPA to assist in spreading the particles around the interface. The particle solution is sonicated for >15 min immediately before use to break up any aggregated particles. Five microliters of the solution is added dropwise to a flat air-water and allowed to spread for 15 min. The entire setup is sealed in a form-fitted plastic box with an additional aqueous reservoir to provide humidity control during the measurements. Fifteen minutes after the addition of the particle solution, the fluid interface cannot be seen to change over time due to evaporation. Interferograms are captured using an upright microscope (Nikon FN1) equipped with a  $50\times$  Mirau objective and a CMOS image sensor (Nikon DS-Fi3) following the protocol outlined in ref<sup>13</sup>. Briefly, the sample is illuminated at  $2\times$  zoom using white light passed through a  $575 \pm 25 \text{ nm}$  band-pass filter. A piezo-controlled nano-drive (MCL Nano-Z) is used to move the objective 36 nm between each 70 ms exposure. In this way 32 interferograms spaced by  $\lambda/16 \text{ nm}$  are captured. These interferograms are analyzed to create a map of relative height around the surface of the particle using phase-shift interferometry<sup>13</sup>. The interferometry analysis protocols account for any remnant macroscopic curvature of the interface and in-plane motion (translation/rotation) of the particle in order to achieve height maps with  $\pm 1 \text{ nm}$  resolution. While a single representative interferogram is shown for each case in Fig 2a, subsequent data is an average of the results from at least five different particles for each case.

### AUTHOR INFORMATION

#### Corresponding Author

Peter J. Beltramo – Department of Chemical Engineering, University of Massachusetts Amherst, Amherst, Massachusetts 01003, United States; ORCID: [orcid.org/0000-0003-3837-4457](https://orcid.org/0000-0003-3837-4457); Email: [pbeltramo@umass.edu](mailto:pbeltramo@umass.edu)

#### Notes

The authors declare no competing financial interests.

### ACKNOWLEDGMENT

Particle characterization was performed at the UMass Amherst Center for Electron Microscopy, and the authors thank Dr. Alexander Ribbe for assistance with SEM and AFM. Funding for this work was provided by the National Science Foundation under award no. CBET-2232579.

### REFERENCES

- (1) Rahman, M. A.; Beltramo, P. J. *Rough Colloids at Fluid Interfaces: From Fundamental Science to Applications*. *Front Phys* 2023, 11, 1248706. <https://doi.org/10.3389/FPHY.2023.1248706/BIBTEX>.
- (2) Aguirre, M.; Ballard, N.; Gonzalez, E.; Hamzehlou, S.; Sardon, H.; Calderon, M.; Paulis, M.; Tomovska, R.; Dupin, D.; Bean, R. H.; Long, T. E.; Leiza, J. R.; Asua, J. M. *Polymer Colloids: Current Challenges, Emerging Applications, and New Developments*. *Macromolecules* 2023, 56 (7), 2579–2607. [https://doi.org/10.1021/ACS.MACROMOL.3C00108/ASSET/IMAGES/LARGE/MA3C00108\\_0001.JPEG](https://doi.org/10.1021/ACS.MACROMOL.3C00108/ASSET/IMAGES/LARGE/MA3C00108_0001.JPEG).
- (3) Zhang, J.; Sun, Z.; Yang, B. *Self-Assembly of Photonic Crystals from Polymer Colloids*. *Curr Opin Colloid Interface Sci* 2009, 14 (2), 103–114. <https://doi.org/10.1016/J.COCIS.2008.09.001>.
- (4) Guzmán, E.; Martínez-Pedrero, F.; Calero, C.; Maestro, A.; Ortega, F.; Rubio, R. G. *A Broad Perspective to Particle-Laden Fluid Interfaces Systems: From Chemically Homogeneous Particles to Active Colloids*. *Adv Colloid Interface Sci* 2022, 302, 102620. <https://doi.org/10.1016/J.CIS.2022.102620>.
- (5) Stamou, D.; Duschl, C.; Johannsmann, D. *Long-Range Attraction between Colloidal Spheres at the Air-Water Interface: The Consequence of an Irregular Meniscus*. *Phys Rev E* 2000, 62 (4), 5263. <https://doi.org/10.1103/PhysRevE.62.5263>.
- (6) III. *An Essay on the Cohesion of Fluids*. *Philos Trans R Soc Lond* 1805, 95, 65–87. <https://doi.org/10.1098/RSTL.1805.0005>.
- (7) Trevenen, S.; Rahman, M. A.; Hamilton, H. S. C.; Ribbe, A. E.; Bradley, L. C.; Beltramo, P. J. *Nanoscale Porosity in Microellipsoids Cloaks Interparticle Capillary Attraction at Fluid Interfaces*. *ACS Nano* 2023, 17 (12), 11892–11904. <https://doi.org/10.1021/ACS.NANO.3C03301>.
- (8) Loudet, J. C.; Alsayed, A. M.; Zhang, J.; Yodh, A. G. *Capillary Interactions between Anisotropic Colloidal Particles*. *Phys Rev Lett* 2005, 94 (1), 2–5. <https://doi.org/10.1103/PhysRevLett.94.018301>.
- (9) Danov, K. D.; Kralchevsky, P. A.; Naydenov, B. N.; Brenn, G. *Interactions between Particles with an Undulated Contact Line at a Fluid Interface: Capillary Multipoles of Arbitrary Order*. *J Colloid Interface Sci* 2005, 287 (1), 121–134. <https://doi.org/10.1016/j.jcis.2005.01.079>.
- (10) San-Miguel, A.; Behrens, S. H. *Influence of Nanoscale Particle Roughness on the Stability of Pickering Emulsions*. *Langmuir* 2012, 28 (33), 12038–12043. <https://doi.org/10.1021/la302224v>.
- (11) Zanini, M.; Marschelke, C.; Anachkov, S. E.; Marini, E.; Synytska, A.; Isa, L. *Universal Emulsion Stabilization from the Arrested Adsorption of Rough Particles at Liquid-Liquid Interfaces*. *Nature Communications* 2017 8:1 2017, 8 (1), 1–9. <https://doi.org/10.1038/ncomms15701>.
- (12) Loudet, J. C.; Pouligny, B. *How Do Mosquito Eggs Self-Assemble on the Water Surface?* *Eur Phys J E Soft Matter* 2011, 34 (8). <https://doi.org/10.1140/EPJE/I2011-11076-9>.
- (13) Trevenen, S.; Beltramo, P. J. *Mirau Interferometry of Fluid Interfaces Deformed by Colloids under the Influence of External Fields*. *Review of Scientific Instruments* 2022, 93 (7), 73701. <https://doi.org/10.1063/5.0092135/2848877>.
- (14) Madivala, B.; Fransaeer, J.; Vermant, J. *Self-Assembly and Rheology of Ellipsoidal Particles at Interfaces*. *Langmuir* 2009, 25 (5), 2718–2728. <https://doi.org/10.1021/la803554u>.
- (15) Beltramo, P. J.; Gupta, M.; Alicke, A.; Liascukiene, I.; Gunes, D. Z.; Baroud, C. N.; Vermant, J. *Arresting Dissolution by Interfacial Rheology Design*. *Proceedings of the Nation-*

al Academy of Sciences 2017, 114 (39), 201705181.  
<https://doi.org/10.1073/pnas.1705181114>.

(16) Madivala, B.; Vandebriel, S.; Fransaer, J.; Vermant, J. Exploiting Particle Shape in Solid Stabilized Emulsions. *Soft Matter* 2009, 5 (8), 1717–1727.  
<https://doi.org/10.1039/B816680C>.

(17) Li, X.; Gilchrist, J. F. Large-Area Nanoparticle Films by Continuous Automated Langmuir-Blodgett Assembly and Deposition. *Langmuir* 2016, 32 (5), 1220–1226.  
<https://doi.org/10.1021/ACS.LANGMUIR.5B03760>/ASSET/IMAGES/LARGE/LA-2015-03760\_0007.JPG.

(18) Parchine, M.; McGrath, J.; Bardosova, M.; Pemble, M. E. Large Area 2D and 3D Colloidal Photonic Crystals Fabricated by a Roll-to-Roll Langmuir-Blodgett Method. *Langmuir* 2016, 32 (23), 5862–5869.  
<https://doi.org/10.1021/ACS.LANGMUIR.6B01242>/ASSET/IMAGES/LARGE/LA-2016-01242\_0011.JPG.

(19) Maria Bardosova, B.; Pemble, M. E.; Povey, I. M.; Tredgold, R. H. The Langmuir-Blodgett Approach to Making Colloidal Photonic Crystals from Silica Spheres. *Advanced Materials* 2010, 22 (29), 3104–3124.  
<https://doi.org/10.1002/ADMA.200903708>.

(20) Rahman, M. A.; Turner, T.; Hamilton, H. S. C.; Bradley, L. C.; Beltramo, P. J. Engineering the Surface Patchiness and Topography of Polystyrene Colloids: From Spheres to Ellipsoids. *J Colloid Interface Sci* 2023, 652, 82–94.  
<https://doi.org/10.1016/J.JCIS.2023.08.083>.

(21) Trevenen, S.; Beltramo, P. J. Gradient Stretching to Produce Variable Aspect Ratio Colloidal Ellipsoids. *J Colloid Interface Sci* 2021, 583, 385–393.  
<https://doi.org/10.1016/j.jcis.2020.09.065>.

(22) Lehle, H.; Noruzifar, E.; Oettel, M. Ellipsoidal Particles at Fluid Interfaces. *European Physical Journal E* 2008, 26 (1–2), 151–160. <https://doi.org/10.1140/epje/i2007-10314-1>.

(23) Wang, A.; McGorty, R.; Kaz, D. M.; Manoharan, V. N. Contact-Line Pinning Controls How Quickly Colloidal Particles Equilibrate with Liquid Interfaces. *Soft Matter* 2016, 12 (43), 8958–8967. <https://doi.org/10.1039/C6SM01690A>.

(24) Coertjens, S.; Dier, R. De; Moldenaers, P.; Isa, L.; Vermant, J. Adsorption of Ellipsoidal Particles at Liquid-Liquid Interfaces. *Langmuir* 2017, 33 (11), 2689–2697.  
<https://doi.org/10.1021/acs.langmuir.6b03534>.

(25) Dasgupta, S.; Katava, M.; Faraj, M.; Auth, T.; Gompper, G. Capillary Assembly of Microscale Ellipsoidal, Cuboidal, and Spherical Particles at Interfaces. *Langmuir* 2014, 30 (40), 11873–11882. <https://doi.org/10.1021/la502627h>.

(26) Nonomura, Y.; Komura, S.; Tsujii, K. Adsorption of Microstructured Particles at Liquid-Liquid Interfaces. *Journal of Physical Chemistry B* 2006, 110 (26), 13124–13129. [https://doi.org/10.1021/JP0617017/SUPPL\\_FILE/JP0617017SI20060509\\_082130.PDF](https://doi.org/10.1021/JP0617017/SUPPL_FILE/JP0617017SI20060509_082130.PDF).

(27) Loudet, J. C.; Yodh, A. G.; Pouligny, B. Wetting and Contact Lines of Micrometer-Sized Ellipsoids. *Phys Rev Lett* 2006, 97 (1), 1–4.  
<https://doi.org/10.1103/PhysRevLett.97.018304>.

(28) Nonomura, Y.; Komura, S.; Tsujii, K. Surface-Active Particles with Microstructured Surfaces. *Langmuir* 2005, 21 (21), 9409–9411.  
<https://doi.org/10.1021/LA051816M>/ASSET/IMAGES/MEDIUM/LA051816MN00001.GIF.

(29) Paunov, V. N. Novel Method for Determining the Three-Phase Contact Angle of Colloid Particles Adsorbed at Air–Water and Oil–Water Interfaces. *Langmuir* 2003, 19 (19), 7970–7976. <https://doi.org/10.1021/LA0347509>.

(30) Nečas, D.; Klapetek, P. Gwyddion: An Open-Source Software for SPM Data Analysis. *Central European Journal of Physics* 2012, 10 (1), 181–188.  
<https://doi.org/10.2478/S11534-011-0096-2>/MACHINEREADABLECITATION/RIS.

(31) Beton, J. G.; Moorehead, R.; Helfmann, L.; Gray, R.; Hoogenboom, B. W.; Joseph, A. P.; Topf, M.; Pyne, A. L. B. TopoStats – A Program for Automated Tracing of Biomolecules from AFM Images. *Methods* 2021, 193, 68–79.  
<https://doi.org/10.1016/J.YMETH.2021.01.008>.

# TOC graphic

---

